International Journal of Microwave and Wireless Technologies, 2013, 5(2), 179–186. © Cambridge University Press and the European Microwave Association, 2013
doi:10.1017/S1759078713000214

RESEARCH PAPER

Ideal amplification of broadband signals

RON MCCALLISTER

This paper describes a digital signal processing (DSP) method for achieving "ideal" amplification, maximizing both the average output signal power and power-added-efficiency for any signal waveform and any power amplifier (PA) transfer characteristic. Detailed algorithms are described for optimally accomplishing peak reduction (PR), predistortion (PD) linearization, and integration of these DSP techniques with envelope tracking PAs. Hardware characterization results validate the theories of PD and PR operation.

Keywords: Nonlinearity, Power-added-efficiency, Peak-to-average ratio, Power amplifiers, Predistortion, Spectral regrowth, Envelope tracking

Received 27 September 2012; Revised 15 February 2013

I. INTRODUCTION

Power amplification of narrowband signals using a radiofrequency (RF) choke bias network and lookup-table (LUT) linearization offers excellent results, especially when the signal exhibits low peak-to-average (power) ratio (PAR) values. However, wide signal bandwidths with high PAR values present unique power amplification challenges. Wireless data links need maximum average transmitted signal power to maximize link capacity, and maximum amplifier power-added efficiency (PAE) is needed to minimize battery/supply power drain. How can we satisfy these goals for broadband signals? "Ideal amplification" (IA) achieves both objectives simultaneously, for all amplifier transfer characteristics and all signal waveforms.

IA requires optimal solution of three problems: (1) peak reduction (PR) shaping of the probability density function (pdf) of the signal magnitude; (2) predistortion (PD) of the signal waveform to effectively linearize the nonlinear amplifier transfer characteristic; and (3) effectively integrating those solutions with an envelope-tracking (ET) power amplifier (PA).

This requires: (1) precluding the signal magnitude pdf tail ("cause of spectral regrowth" in Fig. 1) from exceeding the amplifier's linear range and (2) altering the amplifier transfer characteristic to be piecewise-linear, as depicted in Fig. 1 [1]. IA requires that these goals be simultaneously achieved and that amplifier PAE be maximized by ideal integration with an ET PA. Each goal is addressed in subsequent parts of this paper.

II. SIGNAL PR

Hundreds of published papers have addressed various PAR reduction approaches over recent decades. The most common [2, 3] approach uses iterative removal of a scaled fixed-shape pulse, gradually reducing peaks while meeting out-of-band (OOB) spectral energy constraints. However, superior performance is achievable with far less DSP complexity using the concept of the signal "excursion" waveform. The excursion waveform, $x(t)$, associated with any signal waveform, $s(t)$, and magnitude bound, B, is simply defined as,

$$x(t) \equiv \begin{cases} 0, & |s(t)| \le B, \\ s(t) - B\dfrac{s(t)}{|s(t)|}, & |s(t)| > B. \end{cases} \quad (1)$$

Figure 2 depicts the excursion waveform as a complex function of time.

Subtracting the filtered, scaled, and time-aligned excursion waveform from the signal to accomplish PAR reduction was first described by Armstrong [4], who scaled the filtered excursion to restore peak magnitude. McCallister [5] first applied channel-specific scaling to match excursion energy in each signal channel to that channel's error vector magnitude (EVM) constraint, a necessary condition for minimum PAR. Optimal PR demands that both forms of scaling be simultaneously applied, posing a "chicken-and-egg" challenge.

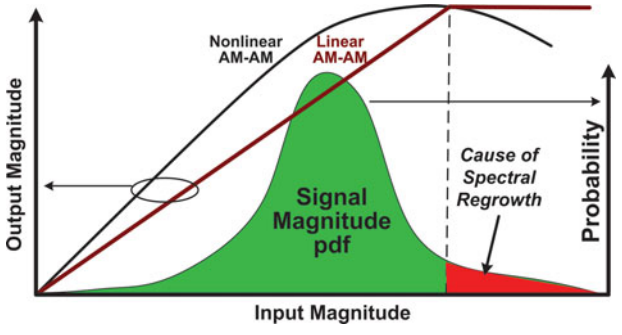


Fig. 1. Spectral regrowth: mechanism and cure.

Crestcom, Inc., Scottsdale, AZ, 85258, USA
Corresponding author:
R. McCallister
Email: ron@crestcominc.com

https://doi.org/10.1017/S1759078713000214 Published online by Cambridge University Press

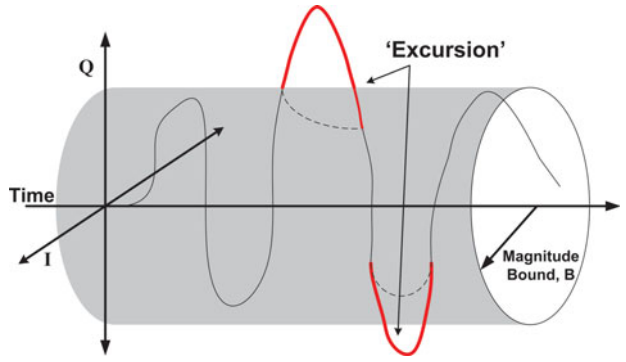


Fig. 2. "Excursion" associated with a complex signal over time.

Dynamic modulation and coding imply dynamic channel EVM values, demanding dynamic scaling of the excursion energy corresponding to each signal channel. Frequency-dependent channel scaling filters the excursion waveform, demanding corresponding time-domain scaling. Finally, dynamic scaling of the excursion waveform alters the excursion energy in each channel. McCallister [6] used automatic-gain-control (AGC) of the excursion energy corresponding to each signal channel to resolve this dilemma, constantly adapting channel scaling to "nudge" excursion channel energy toward its EVM constraint. The channel gain-versus-frequency profile defines a linear filter, from which the required time-domain peak scaling may be readily computed.

A) Optimal PR processing architecture

Figure 3 depicts the optimal PR functional architecture, applicable to all multi-channel signals: non-Orthogonal Frequency division multiplexed (OFDM) (e.g. EV-DO, Rev. C) and OFDM-based (e.g. WiMAX and LTE). Non-OFDM signals use an FFT-based transmultiplexer for channel filtering and scaling; OFDM signals use direct FFT-based processing. Feedback from the channel-specific scaling operation to the time-domain excursion scaling operation is critical to achieve optimal PAR reduction.

Optimal PR processing for OFDM waveforms is simple: real scaling is applied to each excursion FFT according to each channel's EVM constraint, and the time-domain scaling is a simple function of the relative numbers of each EVM value (modulation and code type).

Figure 4 depicts performance obtained using optimal PR processing executed using Field-programmable gate array (FPGA) hardware with a 20 MHz 15-channel QPSK EV-DO Rev. C signal. A 4.75 dB PAR is achieved while satisfying all OOB and EVM constraints, and with DSP complexity that is about 25% of prior PAR reduction art [7].

PR processing yields ~6 dB PAR for typical OFDM (e.g. WiMAX, 802.11ac) signals, achieving low PAR without the

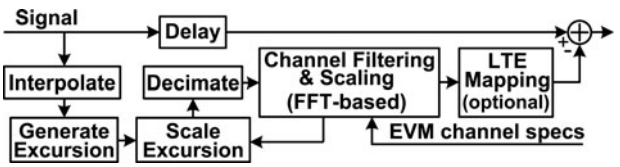


Fig. 3. Optimal PAR reduction functional architecture.

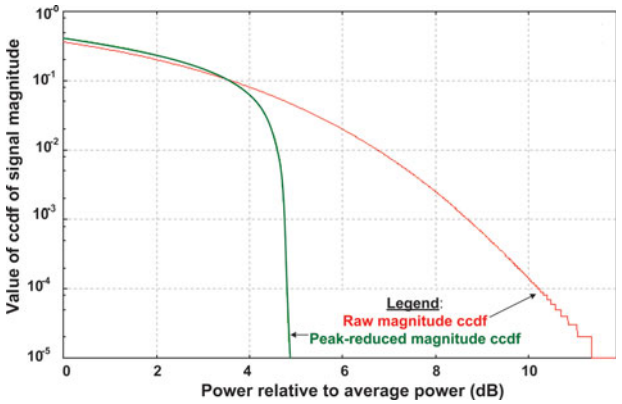


Fig. 4. Multi-channel PR results using FPGA hardware.

orthogonality loss penalty imposed by LTE's precoding transform [8], which can exceed 2 dB. While optimally peak-reduced WiMAX has lower PAR than conventional LTE, our PR processing significantly reduces the PAR of conventional LTE.

B) PAR reduction: nonaggregated LTE

Following verification that MATLAB simulation results matched FPGA PR processing results for 20 MHz 15-channel Rev C EVDO, the PR simulation was used to simply and accurately characterize LTE PR performance. LTE signals were generated based on Myung's published MATLAB LTE simulation code [9]. For single-band LTE transmissions satisfying regulatory spectral mask constraints ($\alpha = 0.25$ root-Nyquist filter), PAR value can be reduced by 3.5 dB for 100% (2.4 dB for 50%) LTE uplinks; Figs 5 and 6 depict LTE magnitude-versus-time and PAR characterizations, respectively.

C) PAR reduction: aggregated-band LTE

For aggregated-band LTE transmission, LTE's 7.6 dB PAR value ($\alpha = 0.25$ root-Nyquist spectrum shaping) is easily reduced by 3 dB for 100% (1.5 dB for 50%) usage. Optimal PAR reduction provides a 70% increase in PA output power

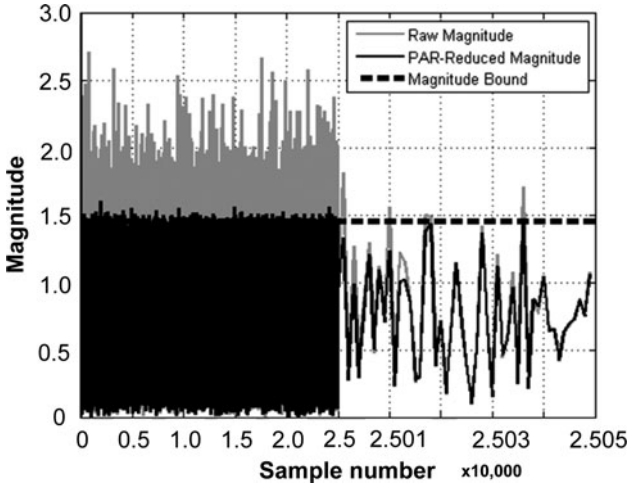


Fig. 5. Single-channel LTE PR using MATLAB simulation.

https://doi.org/10.1017/S1759078713000214 Published online by Cambridge University Press

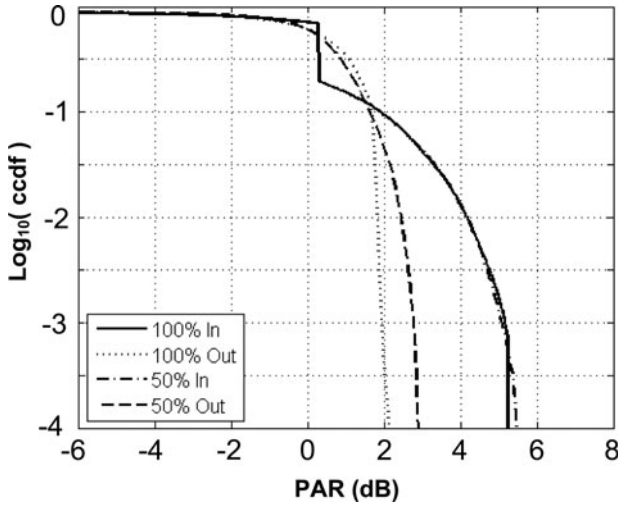


Fig. 6. Single-channel PAR reduction: ccdf curves.

for precisely those high-rate uplinks where PA power is most needed. Figure 7 depicts PAR results for LTE signals in three separate 5 MHz bands spread over a 20 MHz transmission band using ×2 oversampling.

III. PD LINEARIZATION

The second critical technical challenge, PD linearization, has also generated hundreds of technical papers and patents, starting nearly 40 years ago [10] with Weber's PD of the modulation constellation. Least-mean-square (LMS)-based adaptive PD quickly followed [11], then simplification [12] to a magnitude-addressed LUT.

Most recent advances use generalized memory polynomial (GMP) processing [13] to achieve high linearity in Class A operation. While GMP greatly improves linearity, GMP's DSP implementation demands unacceptably high power consumption for cell phone and portable wireless applications to execute GMP's complex DSP operations. GMP's success proved that PA nonlinear energy is deterministic, indicating compensation should be achievable. The very high condition numbers associated with the GMP matrices clearly indicated that this method uses an inefficient model; this suggested that a physics-based PA model might yield comparable results while requiring far simpler DSP.

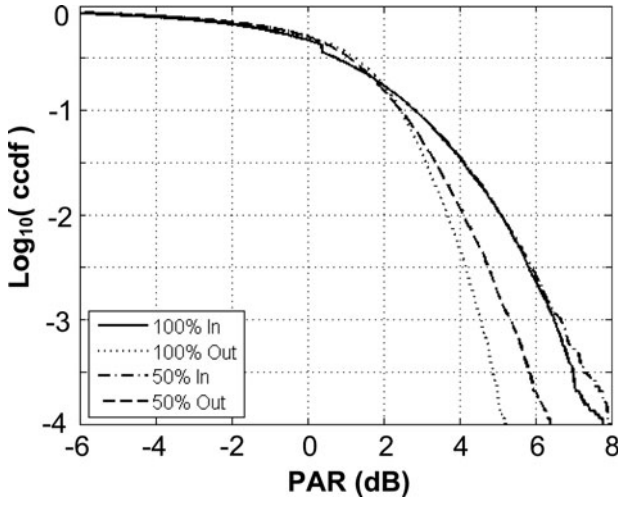


Fig. 7. Multi-channel PAR reduction MATLAB results.

A) Physical amplification model

The simplest physical single-transistor PA model assumes the existence of a nonlinear conductance manifold, where the conductance is a nonlinear function of both the control (gate) voltage and the voltage across the PA. Figure 8 depicts a conductance manifold [14] for a GaN PA device.

Assuming a simple RF choke feed in the output bias network, the PA circuit model is depicted in Fig. 9. Supply voltage, V_{dd}, supplies charge to the circuit, and in response to variations in input RF voltage, V_{gs}, the dynamic conductance routes RF current to the resistive load through the output matching network (OMN). If the choke impedance is much smaller than the inverse of the PA conductance, we may accurately approximate the current as the product of the supply voltage and the PA conductivity – the basis for the pedagogical tool of a (non-existent) nonlinear PA "current source". The PA generates an effective "current manifold", which is a nonlinear function of both gate and drain voltages.

Gate voltage, $v_{gs}(t)$, may be represented as a sinusoid modulated by arbitrary magnitude, $M(t)$, and phase, $\Theta(t)$

$$v_{gs}(t) \equiv M(t)\cos[\omega_c t + \theta(t)]. \quad (2)$$

Model the amplifier current as having power-series dependence on gate voltage, with the series coefficients, a_n, reflecting

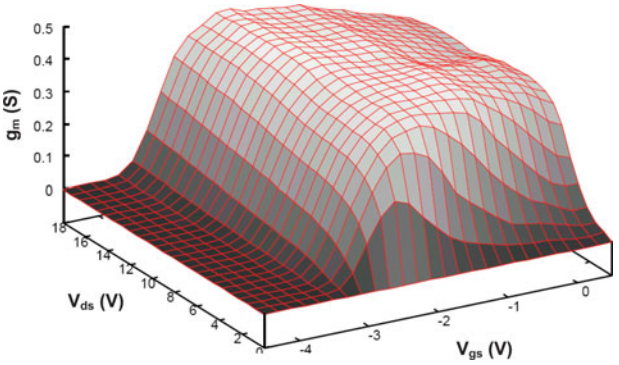


Fig. 8. GaN conductance manifold.

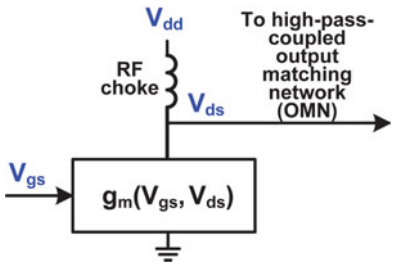


Fig. 9. Simple physical model of PA circuit.

https://doi.org/10.1017/S1759078713000214 Published online by Cambridge University Press

the current manifold's dependence on V_{ds}.

$$i_{ds}(t) \equiv \sum_{n=1}^{N} a_n[v_{ds}(t)]v_{gs}^n(t). \quad (3)$$

Exploiting the binomial theorem yields,

$$v_{gs}^n(t) = \left(\frac{M^n(t)}{2^n}\right)\mathrm{Re}\left\{\sum_{k=0}^{n}\binom{n}{k}\left[e^{j\Theta(t)}\right]^k\left[e^{-j\Theta(t)}\right]^{n-k}e^{j\omega_c(2k-n)t}\right\}. \quad (4)$$

The video component of $i_{ds}(t)$ is then seen to be

$$i_{ds,\,video}(t) = \left[\sum_{even_n}^{N}\frac{a_n[v_{ds}(t)]}{2^n}\binom{n}{\frac{n-1}{2}}\right]M^n(t). \quad (5)$$

Similar analysis describes RF current at all harmonics. These components modulate voltage across the amplifier, generating spurious nonlinear RF energy, and must be eliminated or compensated to achieve linear amplification.

Saleh [15] prescribed minimizing the impedance at video and all RF harmonics to minimize the distortion induced by these spurious currents. The logic is compelling: eliminate the impedances and the voltage-induced gain variations disappear. Eliminating the impedance at RF harmonics is readily accomplished using simple LC traps. Assuming resistive matching (i.e. negligibly dispersive RF passband impedance), a simple LUT linearizer [12] readily compensates for AM–AM and AM–PM associated with the nonlinear passband current, leaving only the problematic video impedance.

B) Video impedance coping strategies

For the past two decades, designers have tried to minimize impact of RF "choke" inductance, whose linearly increasing video impedance induces intractable PA gain nonlinearity for broadband signals. The challenge is to minimize video band bias impedance, while assuring RF passband (bias) impedance greatly exceeds RF passband OMN impedance – lest wasted RF power decrease PAE. To this end, resonance [16], multi-pole high-pass networks and arrays of spaced-resonance shunt capacitors [17] have been used. These strategies induce resonant voltages precluding operation beyond 1 dB compression points, and impose severe constraints on tuning and manufacturing processes.

Our alternate strategy adaptively compensates for the nonlinear PA gain variation caused by gate and drain "choke" inductances. Amplifier gain is a nonlinear function of both $v_{gs}(t)$ and $v_{ds}(t)$.

$$g_m(t) = f\big(v_{gs}(t), v_{ds}(t)\big). \quad (6)$$

But from Fig. 9, we see that $v_{ds}(t)$ is a nonlinear function of both signal magnitude and its time derivative.

$$V_{ds}(t) = V_{dd} - L_b\dot{M}(t)\frac{\mathrm{d}i_{ds,video}[M(t)]}{\mathrm{d}t}. \quad (7)$$

Combining (2), (6), and (7) leads to the key conclusion that amplifier gain must be a nonlinear function of both signal magnitude and its time derivative. Although the memoryless nonlinearity is unknown, we can simply exploit the powerful LMS algorithm to drive the contents of a suitable LUT to optimal gain compensation – easily done when the LUT address space spans both signal magnitude and its time derivative.

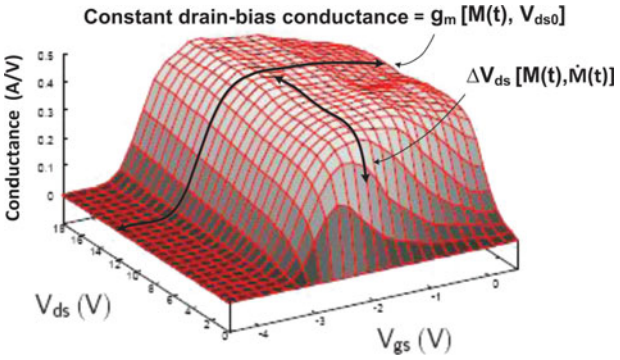


Fig. 10. Conductance manifold dynamic gain components.

Conventional magnitude-based LMS linearizers cannot correct $\dot{M}$-induced gain nonlinearities, since magnitude and its derivative are uncorrelated for all band-limited signals.

$$\langle M(t)\dot{M}(t)\rangle = \langle M(t)\lim_{\tau\to 0}\left\{\frac{M(t+\tau)-M(t)}{\tau}\right\}\rangle. \quad (8)$$

Interchanging the expectation, $\langle\,\rangle$, and limit operators, we find this correlation equals the derivative of the magnitude autocorrelation function evaluated at zero.

$$\langle M(t)\dot{M}(t)\rangle = \underset{\tau\to 0}{Lim}\left\{\frac{R_M(t+\tau)-R_M(t)}{\tau}\right\} = \dot{R}_M(0) \approx 0. \quad (9)$$

Therefore, $\dot{M}$-induced gain errors cannot generate adaptive correction in conventional M-only-based LMS linearizers.

Our new amplification model describes movement over the conductivity/current manifold as no longer along only iso-V_{ds} contours, but now including a dynamic component of movement transverse to those iso-V_{ds} contours. Composite movement, and amplifier gain, is a function of both magnitude and its derivative, as depicted in Fig. 10.

C) Proposed "memory" nonlinearity compensation

Video current is a function of magnitude, so the voltage generated by resistive and inductive video impedance must be a nonlinear function of magnitude and its derivative; resulting PA gain variation must then be a function of both parameters. Although nominal nonlinear gain is a function of only magnitude, composite PA gain must be a memoryless function of magnitude, M, and its derivative, $\dot{M}$. We simply augment the LUT address, appending to the magnitude bits those bits representing the (scaled) derivative of the magnitude as depicted in Fig. 11.

This linearizer compensates for video inductance, and can also accommodate dynamic variation of drain (and gate) bias,

https://doi.org/10.1017/S1759078713000214 Published online by Cambridge University Press

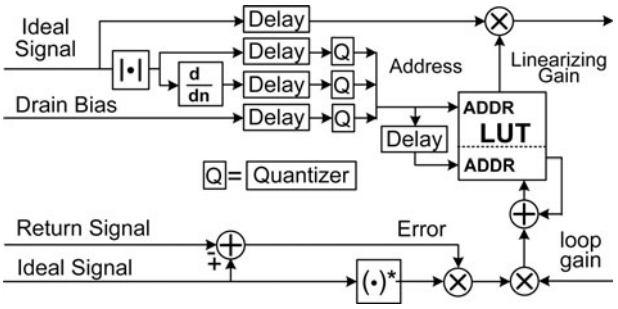


Fig. 11. LUT-based PA linearizer architecture.

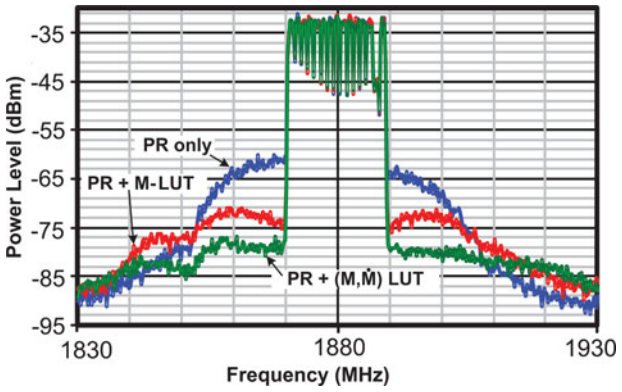


Fig. 13. Comparative linearized PA output spectra.

as shown. Its simplicity is attributable to our viewing amplification as resulting from signal-driven movement over a nonlinear conductance/current manifold.

IV. EXPERIMENTAL RESULTS

A) Hardware system description and experimental results

The demonstration system depicted in Fig. 12 was used to evaluate the validity of the PR and PD concepts and architectures previously described. This system has been used to evaluate performance using a variety of PA technologies, including LDMOS, GaN, and pHEMT.

The return demodulator depicted in Fig. 12 uses a simple bandpass filter centered on the RF passband and wide enough to pass ~6× the signal bandwidth, then coherent subsampling [18] using a SiGe sample-and-hold to extract a precise replica of the transmitted signal.

An Avago pHEMT PA (ATF-501P8 transistor) was used to perform the experiment described below. A 20 MHz RF signal centered at 1.885 GHz and consisting of 15 parallel EV-DO CDMA signals (random data bits) was generated by a DSP Board FPGA. Figure 13 depicts the comparative output spectra when using PR but no linearization (blue top trace), conventional M-based LUT linearization (red middle trace), and finally, LUT linearization based on both M and Ṁ (green bottom trace). Compensating for nonlinear gain induced by the derivative of magnitude significantly enhances linearization.

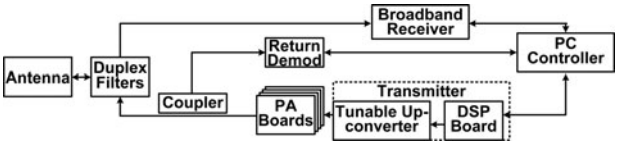


Fig. 12. RF Transceiver used to evaluate ideal linearization.

Further validation for our PA model is provided by examination of the gain values in the LUT after the LMS algorithm has converged to stable values. To speed convergence and emphasize the differences we used two parallel LUTs, one conventional and the other (M, Ṁ). Figure 14 depicts two views of the real part of (M, Ṁ) LUT gain versus both M and Ṁ; clearly, optimal gain compensation is strongly a function of both M and Ṁ. For comparison, conventional M-based LUT gain magnitudes are less than unity. These results prove that the "RF choke" gain nonlinearity mechanism is significant and that the solution in Fig. 11 is viable and effective.

PA output power is constrained by a regulatory spectral mask constraining OOB signal power as depicted in Fig. 15; operating outside the PA linear region generates OOB power violating this mask and requiring increased PA backoff. The average transmit power increases achievable while satisfying the spectral mask are a direct measure of the value of PR and PD processing. (Note: channel scaling automatically adjusts, as depicted in Fig. 3, to ensure that EVM specifications remain satisfied.)

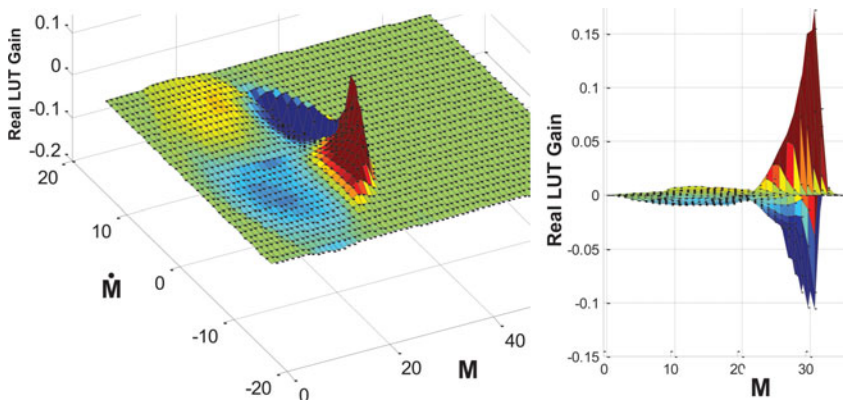


Fig. 14. LUT optimal (M, Ṁ) gain compensation.

https://doi.org/10.1017/S1759078713000214 Published online by Cambridge University Press

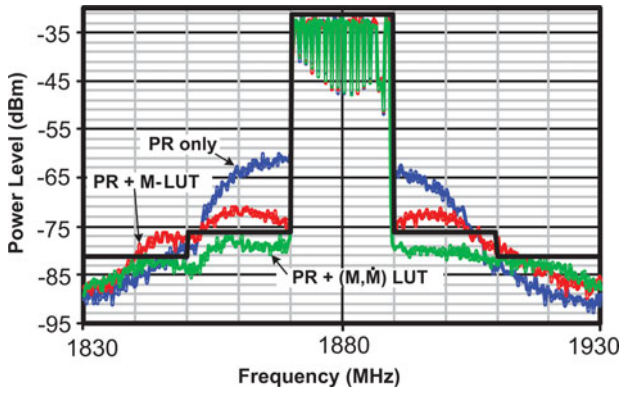


Fig. 15. Signal power versus typical regulatory spectral mask.

Table 1. Measured increase in average transmit power (dB).

Peak-reduction only	3.6
Peak-reduction and M-LUT	6.5
Peak-reduction and (M, Ṁ) LUT	**7.8**

Compared with operation with neither PR nor linearization, experimental results in Table 1 demonstrate that the enhanced PR and PD algorithms described in this paper substantially increase average PA transmit power.

Our results show that the PD in Fig. 12 significantly improves pHEMT PA linearization and validate both the hypothesized nonlinearity mechanism and the efficacy of our solution. Combined, these simple DSP techniques increased average transmit power six-fold (7.8 dB). Enhanced PR and PD DSP algorithms clearly offer substantial cost and power savings benefits for products using broadband wireless transmitters, such as those supporting video telephony and cloud computing applications.

B) Interpretation of experimental results

We may reasonably speculate on the benefits this new PD might offer for CMOS and LDMOS PAs. Figure 16 depicts normalized magnitude transfer characteristics for both pHEMT and CMOS PA devices. pHEMT PAs exhibit linearity

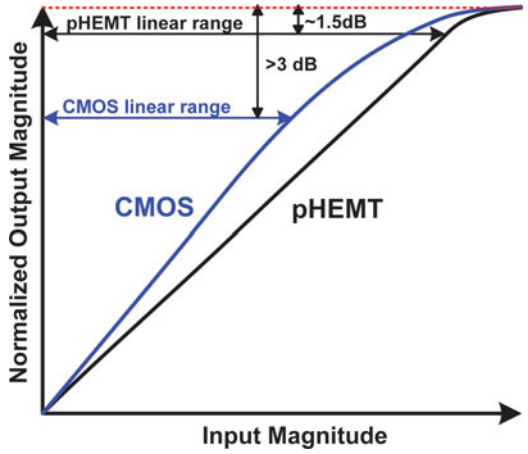


Fig. 16. Normalized magnitude PA transfer characteristics.

to near-saturation; CMOS PAs exhibits more gradual nonlinearity, with several dB between the 1 dB compression point and saturation. Since the (M, Ṁ) LUT demonstrated ability to more completely linearize the pHEMT device, increasing linear power by 1.3 dB, we speculate that the (M, Ṁ) LUT may increase the average linear power from a CMOS PA by several dB.

Such an increase could make it possible to transmit 4G broadband signals using CMOS PAs, making it practical to develop fully integrated multi-band RF transmitters for cellular band applications, offering similar manufacturing and cost efficiencies as current multi-band WiFi products. Future research will explore this possibility by evaluating these improved PR and PD techniques with CMOS PAs.

V. IMPLEMENTATION COMPLEXITY ASSESSMENT

The PAR reduction technique is predominantly FFT-based, so the methodology used to design a reconfigurable FFT chip [19] permits accurate estimation of its implementation complexity. This methodology yields an estimated PAR reduction complexity of ~0.77 mm² and ~16 mW power for a 20 MHz band with a 22 nm CMOS process. Implementation complexity estimation for linearization based on the (M, Ṁ) LUT is currently in progress.

VI. SYNERGIES WITH ET

Significant progress has been made since 1995 [20] enhancing PA power efficiency by adaptively varying bias (V_{DS}) voltage. If V_{DS} is adjusted so that all signal peaks remain within the PA's linear range, no nonlinear energy is generated; minimum power drain (V_{DS}) over time maximizes PA efficiency. Modern ET PAs demonstrate [21] excellent PAE. The primary driver of ET implementation complexity is the supply voltage tracking bandwidth, B_T [22]; fortunately most efficiency gain is achievable [23] using small (~1%) ratios of B_T to signal bandwidth, B_S.

ET PAs can be improved using a V_{DS} waveform directly responsive to signal peaks, rather than scaling rms signal power. For any B_T value, there is a unique "peak-riding" V_{DS} waveform which just exceeds all signal peaks while minimizing the waveform's rms energy; define that V_{DS} waveform as a bandwidth-optimized peak-riding (BOPR) waveform. Peak-tracking (PT) PAs vary V_{DS} to be BOPR proportional; they enhance efficiency for larger B_T values.

A) Enhanced PR synergy with ET

Figure 17 depicts an example of a PR operation using a constant magnitude limit (threshold). A constrained-B_T ET PA offers little efficiency improvement; V_{DS} cannot vary quickly enough to track the rapid residual signal changes.

Optimal synergy between PR and ET requires that the PR magnitude threshold be proportional to the BOPR waveform; PR then generates far less noise coping with the largest peaks, while residual signal peaks are B_T-trackable. BOPR scaling is adaptively reduced until the average noise generated by clipping signal peaks exactly equals the EVM noise budget. ET can track post-PR signal peaks, since the bandwidth of the

https://doi.org/10.1017/S1759078713000214 Published online by Cambridge University Press

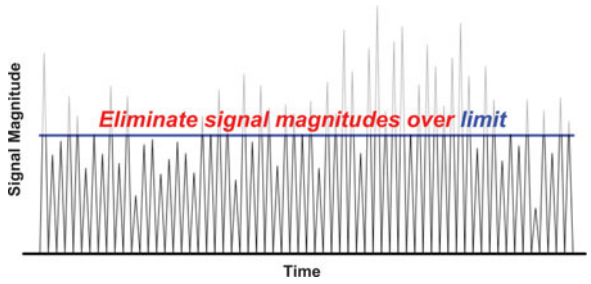


Fig. 17. PR using constant magnitude threshold.

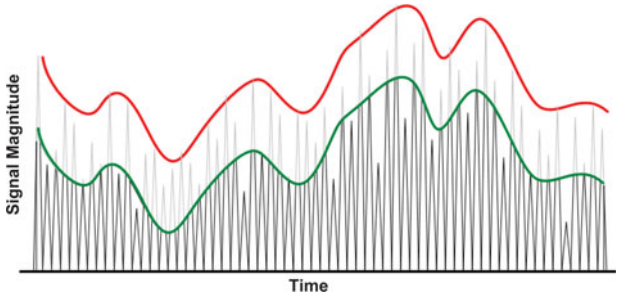


Fig. 18. PR using scaled BOPR for magnitude threshold.

scaled BOPR waveform still equals B_T. Average noise generated clipping signal peaks equals the EVM budget in both cases, but using a scaled version of the BOPR as PR magnitude threshold, as in Fig. 18, significantly enhances PA efficiency.

B) Enhanced PD synergy with ET

Conductivity and gain manifolds associated with MESFET and CMOS PAs [24, slide 10] exhibit significant V_{DS} sensitivity near their 1 dB compression point; Fig. 19 confirms this holds for LDMOS PAs as well [25]. Compensation for gain variation induced by V_{DS} variation is needed to apply ET to such devices whenever effective PD significantly extends their linear range. The LUT-based PD architecture in Fig. 12 compensates for all-gain nonlinearity induced by an arbitrary drain bias (V_{DS}) variation, thus permitting

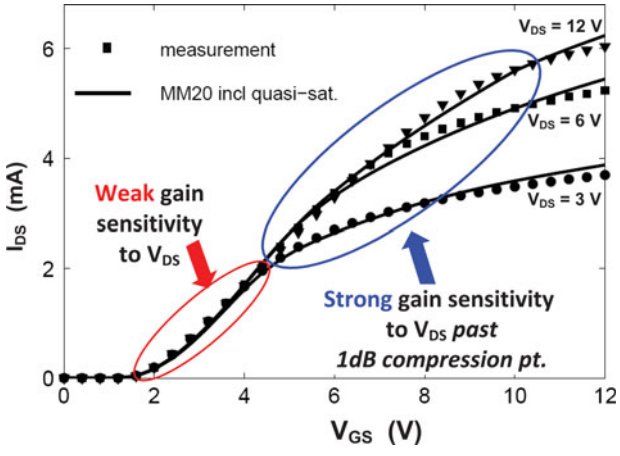


Fig. 19. Gain sensitivity to V_{DS} beyond 1 dB compression point.

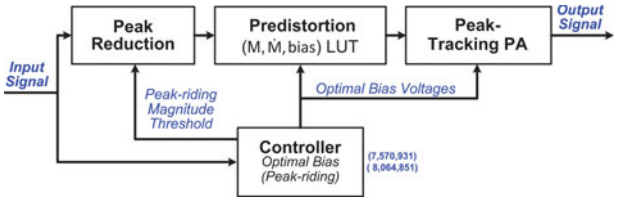


Fig. 20. Integrated IA system architecture.

CMOS ET PA use well beyond the 1 dB compression point with negligible gain nonlinearity induced by V_{DS} variation.

C) Optimal integrated system: PR + PD + ET

Figure 20 depicts the fully integrated version of an IA system. The controller generates the BOPR waveform using known techniques [26] and then supplies it to a processing cascade of PR, PD, and ET PA. This architecture simultaneously maximizes PA output average power and PAE for all signals and all amplifier types. It promises to more than quadruple the average output power from CMOS PAs, so that they may be fully integrated into CMOS transmitter ICs. Such integrated CMOS devices promise multi-band cellular transmitters similar to those currently available for unlicensed band WiFi transmission.

VII. CONCLUSION

Optimal methods for accomplishing both PR and PD for arbitrary broadband signals and amplifiers and a new system architecture that optimally integrates PR, PD and ET PAs have been described. Hardware results validate the proposed broadband PR and PD techniques. Future work will evaluate performance with CMOS PAs, and will incorporate RF traps to eliminate harmonic-induced nonlinearities. Combining optimal PR, PD, and ET processing enables designers of mobile wireless platforms to achieve ideal broadband signal power amplification with minimal implementation complexity; implementation of the solutions described is sufficiently simple and low-power as to be viable for even cell phone market application.

ACKNOWLEDGEMENT

The author gratefully acknowledges contributions by Dr David Hedberg, Dr John Liebetreu, Dr Bruce Cochran, Mr Dan Shearer, Mr Randy Syring, and most significantly, Mr Eric Brombaugh, during the decade-long course of this research.

REFERENCES

[1] McCallister, R. et al.: Radiation hardened modulator ASIC for high data rate communications, in 18th Int. Communication Satellite Systems Conf. Record, Oakland, California, April 10–14, 2000 pp. 229–234.

[2] May, T.; Rohling, H.: Reducing the peak to average power ratio of OFDM and radio transmission systems. IEEE Veh. Technol. Conf., **3** (1998), 2474–2478.

https://doi.org/10.1017/S1759078713000214 Published online by Cambridge University Press

[3] Shearer, D.; Sills, J.: U.S. Patent 6928121, filed September 28, 2001.

[4] Armstrong, J.: New OFDM peak-to-average power reduction scheme, in Proc. of IEEE Vehicular Technology Conf., Rhodes, Greece, May 2001, 756–760.

[5] McCallister, R.: U.S. Patent 7295816, filed December 9, 2003.

[6] McCallister, R.; Brombaugh, E.: U.S. Patent 7783260, filed April 27, 2006.

[7] Texas Instruments GC1115 Crest Factor Reduction Processor, http://www.ti.com/lit/ds/symlink/gc1115.pdf

[8] Ciochina, C.; Sari, H.: A review of OFDMA and single-carrier FDMA, in 2010 European Wireless Conf., 12–15 April 2010, 706–710.

[9] http://www.mathworks.com/matlabcentral/fileexchange/20454-simple-single-carrier-fdma-sc-fdma-simulator

[10] Weber III, W.: The use of TWT amplifiers in m-ary amplitude and phase-shift keying systems. In Proc. of ICC'75, San Francisco, CA, June 1975, pp. 36.17–36.21.

[11] Davis, R.; Boyd, R.: U.S. Patent 4291277, filed May 16, 1979.

[12] Cavers, J.: U.S. Patent 5049832, filed April 20, 1990.

[13] Morgan, D.: A generalized memory polynomial model for digital predistortion of RF power amplifiers. IEEE Trans. Signal Process., **54** (10) 2006, 3852–3860.

[14] http://darwin.bth.rwth-aachen.de/opus3/volltexte/2007/1843/pdf/Chalermwisutkul_Suramate.pdf, p. 84

[15] Saleh, A.; Wazowicz, M.: Efficient linear amplification of varying-envelope signals using FETs with parabolic transfer characteristics. IEEE Trans. Microwav. Theory Tech., **33** (8) (1985), 703–710.

[16] Wisherd, D.: U.S. Patent 5272450, filed June 20, 1991.

[17] Khanifar, A.: U.S. Patent 7034620, filed April 8, 2003.

[18] Ibáñez-Díaz, J. et al.: Nonlinearity estimation in power amplifiers based on subsampled temporal data. IEEE Trans. Instrum. Meas., **54** (10) (2006), 3852–386.

[19] Chia-Hsiang, Y. et al.: Power and area minimization of reconfigurable FFT processors: a 3GPP-LTE example. IEEE J. Solid-State Circuits, **47** (00) (2012), 757–768.

[20] Buoli, C.; Abbiati, A.; Riccardi, D.: Microwave power amplifier with "Envelope Controlled" drain power supply, in 25th European Microwave Conf., September 1995, 31–35.

[21] Kwak, M. et al.: Design of a wideband high-voltage high-efficiency BiCMOS envelope amplifier for micro-base-station RF power amplifiers. IEEE Trans. Microw. Theory Tech., **60** (6) (2012), 1850–1861.

[22] Sahu, B. et al.: System-level requirements of dc-dc converters for dynamic power supplies of power amplifiers, in Proc. of the 2002 IEEE Asia-Pacific Conf. on ASICs, August 6–8, 2002, Taipei, Taiwan, pp. 153–156.

[23] Larson, L. et al.: Intelligent transmitters and power amplifiers for next generation wireless communications, ewh.ieee.org/r6/phoenix/wad/Handouts/LarsonMTTPAtalk.pdf

[24] Angelov, I. et al.: Compact, equivalent circuit models for GaN, SiC, GaAs and CMOS FET, www.mos-ak.org/baltimore/.../02_Angelov_MOS-AK_Baltimore.pdf

[25] Aarts, A. et al.: Compact modeling of high-voltage LDMOS devices including quasi-saturation. IEEE Trans. Electron Devices, **53** (4) (2006), 897–902.

[26] McCallister, R.; Brombaugh, E.: U.S. Patent 7570931, filed June 2, 2000.



Ron McCallister received a degree in Engineering Science from Dartmouth College in 1971, an M.S.E.E from the University of Southern California in 1975, and a Ph.D. degree in communication engineering from Arizona State University in 1981. He co-founded CrestCom, a wireless research firm in 2003, and is its President and CEO. His main research interests are in wireless communication system design and optimization of cellular networks.

https://doi.org/10.1017/S1759078713000214 Published online by Cambridge University Press